


ARTICLE

A specific isoform of Pyd/ZO-1 mediates junctional remodeling and formation of slit diaphragms

Marta Carrasco-Rando, Silvia Prieto-Sánchez, Joaquim Culi, Antonio S. Tutor, and Mar Ruiz-Gómez 

The podocyte slit diaphragm (SD), responsible for blood filtration in vertebrates, is a major target of injury in chronic kidney disease. The damage includes severe morphological changes with destabilization of SDs and their replacement by junctional complexes between abnormally broadened foot processes. In *Drosophila melanogaster*, SDs are present in nephrocytes, which filter the fly's hemolymph. Here, we show that a specific isoform of Polychaetoid/ZO-1, Pyd-P, is essential for *Drosophila* SDs, since, in *pyd* mutants devoid of Pyd-P, SDs do not form and the SD component Dumbfounded accumulates at ectopic septate-like junctions between abnormally aggregated nephrocytes. Reintroduction of Pyd-P leads to junctional remodeling and their progressive normalization toward SDs. This transition requires the coiled-coil domain of Pyd-P and implies formation of nonclathrin vesicles containing SD components and their trafficking to the nephrocyte external membrane, where SDs assemble. Analyses in zebrafish suggest a conserved role for Tjp1a/ZO-1 in promoting junctional remodeling in podocytes.

Introduction

Chronic kidney disease (CKD) is a gradual and irreversible loss of kidney function that often progresses to end-stage renal failure and premature death. Despite current standards of treatment, the incidence of CKD is globally increasing. The early stages of the disease are asymptomatic, leading to diagnosis at an advanced stage characterized by pathological albuminuria and increased mortality (Sanchez-Niño et al., 2017). Therefore, understanding the molecular pathways leading to podocyte injury and developing models to dissect these pathways should facilitate identification of novel therapeutic targets and allow early diagnosis and improved outcomes.

A key target of injury in CKD is the podocyte slit diaphragm (SD; Grahammer et al., 2013). Podocytes are epithelial cells of the renal glomerulus that contribute to the formation of the filtration barrier. They display a specialized morphology with a cell body that projects primary processes, each branching into many foot processes that adhere to the glomerular basement membrane (BM). Foot processes coming from adjacent podocytes interdigitate to fully cover the surface of glomerular capillaries and are joined by modified cell junctions called SDs forming a zipper-like continuous structure that acts as a molecular sieve during the process of blood ultrafiltration that prevents protein loss into urine (Ichimura et al., 2017). The main SD proteins are two members of the immunoglobulin superfamily called nephrin and Neph1 that, through their extracellular regions, maintain

homo- and/or heterophilic interactions that contribute to formation of the molecular filter (Barletta et al., 2003; Gerke et al., 2003). Their cytoplasmic tails associate with additional components of the complex and intracellular adaptors, eliciting signaling cascades fundamental to regulate most aspects of podocyte biology (Grahammer et al., 2013). The stability of the SD is regulated by phosphorylation of its components, which modifies their capacity to associate with intracellular adaptors and affect their recycling (Qin et al., 2009; Hattori et al., 2011). Insults that eliminate or destabilize the SD induce proteinuria that may lead to nephrotic syndrome. Typically, this is accompanied by dramatic morphological changes in podocytes that lead to regression of the foot processes (foot process effacement), as well as loss of SDs and their replacement by occludens-type junctions (Kriz et al., 2013). These modifications have been interpreted as a dedifferentiation process that reverses the events that take place in early podocyte development when occludens junctions migrate to the basal side of the podocyte and are progressively replaced by SDs (Ichimura et al., 2017).

Drosophila melanogaster contains specialized excretory cells called nephrocytes involved in the ultrafiltration of the hemolymph. They have prominent endocytic and exocytic activities, and their morphology reflects their physiological function. Thus, their cell surface is covered by ingressions of the membrane called labyrinthine channels where most of the endocytic

.....
Centro de Biología Molecular Severo Ochoa, Consejo Superior de Investigaciones Científicas and Universidad Autónoma de Madrid, Madrid, Spain.

Correspondence to Mar Ruiz-Gómez: mruiz@cbm.csic.es; S. Prieto-Sánchez's present address is Instituto de Parasitología y Biomedicina López-Neyra, Consejo Superior de Investigaciones Científicas, Granada, Spain; A.S. Tutor's present address is Universidad Europea de Madrid, Madrid, Spain.

© 2019 Carrasco-Rando et al. This article is distributed under the terms of an Attribution–Noncommercial–Share Alike–No Mirror Sites license for the first six months after the publication date (see <http://www.rupress.org/terms/>). After six months it is available under a Creative Commons License (Attribution–Noncommercial–Share Alike 4.0 International license, as described at <https://creativecommons.org/licenses/by-nc-sa/4.0/>).

activity occurs (Aggarwal and King, 1967; Crossley, 1972). The entrance to the channels is limited by the presence of filtration diaphragms strikingly similar to the vertebrate SD and by a BM that surrounds the cell. Dumbfounded (Duf) and Sticks-and-stones (Sns), the orthologues of Neph1 and nephrin, respectively, are the main components of the fly SD, and their inactivation induces gross morphological and functional changes in nephrocytes (Weavers et al., 2009; Zhuang et al., 2009). The morphological changes are reminiscent to podocyte foot process effacement and include the loss of SDs and channels and nephrocyte agglutination associated with appearance of ectopic junctional complexes. Similarities between SDs of vertebrates and flies extend beyond conservation of their components. Thus, protein-protein interactions such as between Polychaetoid (Pyd), the orthologue of ZO-1, and Duf are also conserved, as are the mechanisms that regulate SD stability (Weavers et al., 2009; Tutor et al., 2014). These discoveries allowed the use of nephrocytes to model kidney diseases. As a result, nephrocytes are a powerful tool to identify novel SD components and regulators and unravel the molecular mechanisms responsible for SD stability, damage, and repair (Carrasco-Rando et al., 2015; Na et al., 2015; Helmstädter et al., 2017).

The response of podocytes to damage, which involves an initially reversible junctional remodeling, and the fact that the dissociation of Neph1 and ZO-1 is an early manifestation of damage in animal models of induced nephrosis (Wagner et al., 2008) prompted us to investigate the role played by Pyd/ZO-1, a known cell junction component, in the formation and integrity of the SD. Pyd attenuation in nephrocytes causes smoothening of their surface, suggesting a critical role for Pyd in nephrocyte biology (Zhuang et al., 2009). Moreover, in mice, ZO-1 is required for formation and maintenance of the podocyte filtration barrier (Itoh et al., 2014). In spite of these observations, the molecular mechanism underlying the role of ZO-1/Pyd in SD formation and stability is unknown. Here, we show that in the absence of Pyd, SDs never form and Duf localizes to junctional complexes that appear between abnormally agglutinated nephrocytes. In addition, we find that the isoform required in nephrocytes (Pyd-P) differs from those involved in junctional organization in epithelia. We identify a coiled-coil (CC) domain in Pyd-P as relevant for its function. Furthermore, Pyd appears capable of inducing the transition from septate-like junctions to SDs. Based on these and other findings, we propose a mechanism for Pyd in promoting junctional remodeling. We also find that in zebrafish, attenuation of *tjp1a/zo-1* results in reduction of SDs with a concomitant increase in occludens junctions in broader podocyte processes. This suggests a conserved role of ZO-1 proteins in the junctional remodeling required for SD formation in podocytes and points to ZO-1/Pyd as a potential therapeutic target.

Results

Pyd localizes to the nephrocyte SD and is required for its formation

During *Drosophila* embryonic development, *pyd* is expressed in many tissues (<https://flybase.org>). It is first detected in nephrocytes at embryonic stage 12, later than the onset of Duf and Sns

expression in these precursors (at stage 11; Weavers et al., 2009), which coincides with that of CG32094, an early nephrocyte marker (de Velasco et al., 2006; Fig. S1, A–H). At stage 16, optical sections analyses show that Pyd colocalizes with Duf at regions of the membrane exposed to hemolymph (hereafter referred to as the external membrane; Fig. 1, A and A'; and Video 1). The membrane between apposed nephrocytes accumulates Fasciclin 3 (Fas3) and low levels of Duf (Fig. 1, A and A"). At the ultrastructural level, the nephrocyte external membrane surrounded by BM presents invaginations sealed by SDs (Fig. 1, B'–B'''), whereas no signs of specialized cellular junctions are found at the membranes between adjacent nephrocytes (Fig. 1, B' and B'''), except at the point of contact just underneath the BM (Fig. 1 B'''). In larval nephrocytes, Duf and Pyd colocalize at the nephrocyte external membrane in a fingerprint-like pattern (Fig. 1, C and C') that reflects the location of SDs, sealing the entrance to labyrinthine channels, which now cover the whole nephrocyte surface (Fig. 1 D'). Indeed, immuno-EM reveals that Duf localizes to the SD junction (Weavers et al., 2009; Zhuang et al., 2009), whereas Pyd concentrates at the cytoplasmic side of the SD, as expected for an intracellular adaptor of the complex (Fig. 1, E and E').

Flies homozygous for null alleles of *pyd* are viable and fertile (Djiane et al., 2011); hence, we used them to examine the requirement of Pyd in nephrocytes. In stage 16 *pyd^{ex147}* nephrocytes, Duf localizes to patches at the external membrane and accumulates with Fas3 at cell contacts (Fig. 1, F–F'). However, fingerprint-like distributions are absent suggesting that SDs do not form. Accordingly, transmission EM (TEM) analysis failed to show SDs or deep membrane invaginations (Fig. 1, G' and G'''). As in the WT, the only junctions between adjacent nephrocytes are found at the most external region contacting the BM (Fig. 1 G''). The Duf aggregates found at the external membranes in late *pyd^{ex147}* nephrocytes are transient, since they cannot be detected in larvae (Fig. 1 H). However, Duf still accumulates at membranes located between agglutinated nephrocytes and can be also observed in scarce cytoplasmic vesicles (Fig. 1, H and H'). The lack of SDs was verified by TEM, which also showed thickening of the BM (Fig. 1 I–I-1, compare to Fig. 1 D'), as previously described in *duf* mutants (Weavers et al., 2009). Interestingly, regions of electron-dense material reminiscent of junctional complexes, which accumulate Duf (Fig. 1, J and J'), were often found at cell contacts between agglutinated nephrocytes (Fig. 1 I–I-3). Taken together, our results suggest that during normal development, the SD component Duf transitions from a location in cell contacts to a fingerprint-like pattern in the nephrocyte external membrane. This transition is impaired in *pyd* null mutants, where Duf remains mostly at the cell junctions between abnormally agglutinated nephrocytes. These findings show that, similarly to its vertebrate orthologue ZO-1 (Itoh et al., 2014), Pyd is required for the formation and/or maintenance of SDs.

Mutual requirement of Duf and Pyd for SD development

We further explored the requirement of Pyd for Duf localization and SD formation in nephrocytes by depleting *pyd* for 6 h in late larvae, finding that all remaining Pyd associated with Duf in the

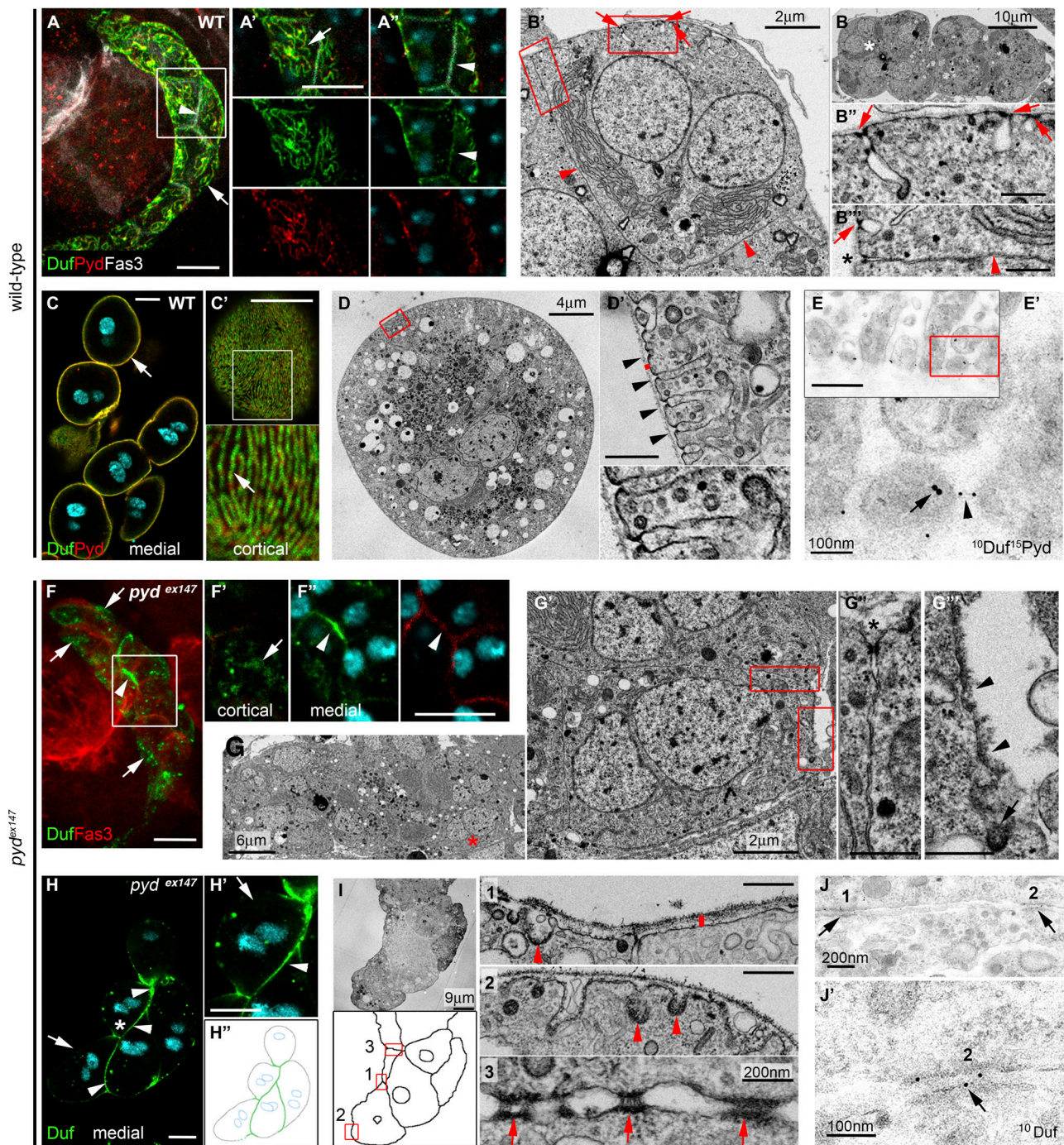


Figure 1. Pyd localizes at the nephrocyte SD and is required for its formation. (A–A'') Confocal images of midtransverse (MT) optical section (A'') or z-projections (A and A') of stage-16 WT nephrocytes stained with the indicated antibodies. Arrows point to Duf/Pyd at SDs and arrowheads to Duf/Fas3 at cell contacts. See also Video 1 and Fig. S1. **(B–B'')** TEM images of MT sections in stage-16 WT nephrocytes. Asterisk in B marks the cell in B'. Arrows point to SDs and arrowheads to cell contacts. Asterisk in B'' marks a junction at the external region of apposed cell membranes ($n = 10$). **(C and C')** Single sections of WT larval nephrocytes stained for Duf, Pyd, and DAPI (cyan). Arrow points to Duf/Pyd at the external membrane (C) with a fingerprint-like distribution (C'; $n = 129$ nephrocytes [N]/12 strings [S]). **(D and D')** TEM images of a WT larval nephrocyte; arrowheads point to SDs, and the height of the red bar indicates the width of the BM ($n = 24$). **(E and E')** TEM images of a larval nephrocyte immunogold-stained for Duf and Pyd ($n = 3$ independent experiments). Duf localizes at the SD junction (arrowhead) and Pyd at the SD cytoplasmic side (arrow). **(F–F'')** z-projection (F) and single sections (F' and F'') of stage-16 *pyd^{Ex147}* nephrocytes stained for Duf and Fas3 ($n = 231$ N). Arrows point to Duf at external patches and arrowheads to Duf/Fas3 at cell contacts. **(G–G'')** TEM images of stage-16 *pyd^{Ex147}* nephrocytes. Asterisk in G' marks a cell junction; arrowheads in G'' point to the plasma membrane lacking SDs and the arrow to a clathrin-coated pit. The red asterisk marks the cell shown in G' ($n = 25$). **(H–H'')** MT sections and cartoon of larval *pyd^{Ex147}* nephrocytes stained for Duf. The asterisk points to the cell shown in H', arrowheads to Duf at cell contacts, and arrows to the external membrane lacking Duf ($n = 83$ N/8S). **(I)** TEM images and cartoon of larval *pyd^{Ex147}* nephrocytes. Note the absence of SDs and the presence of clathrin-coated pits (arrowheads) and junctional complexes between nephrocytes (arrows). The bar denotes the width of the BM (compare to D') and the squares the regions magnified in nearby panels. **(J and J')** Immunoelectron micrographs of *pyd*-silenced larval nephrocytes stained for Duf. Arrows point to Duf at junctional complexes. Unless otherwise indicated, white and black scale bars represent 10 μ m and 500 nm, respectively.

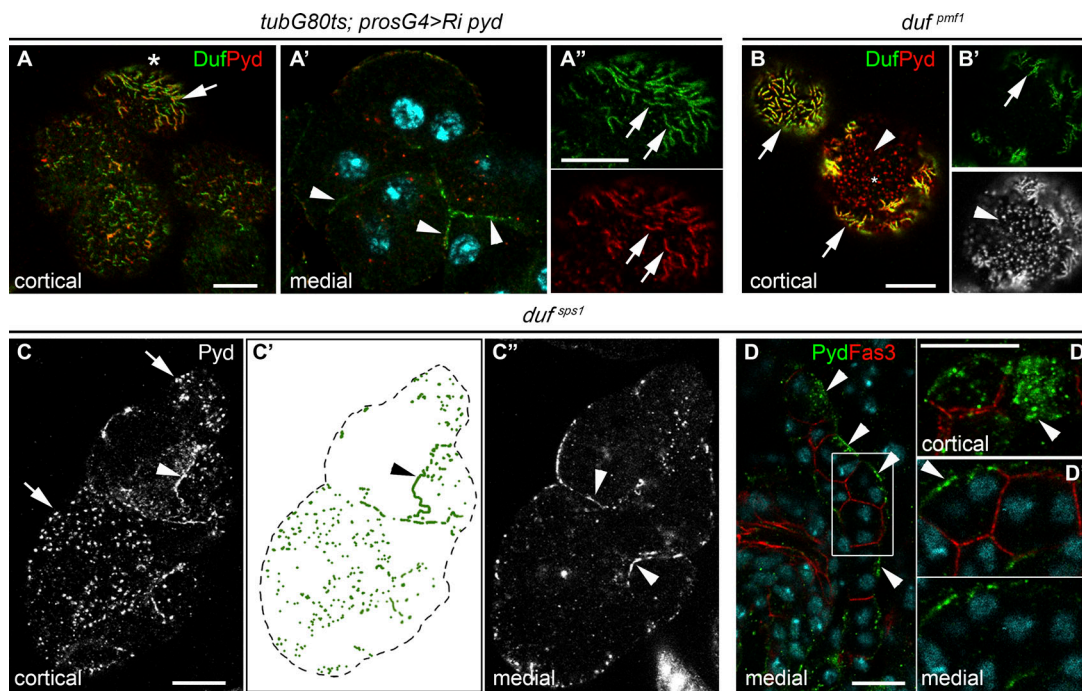


Figure 2. **Duf and Pyd depend on each other to localize at SDs.** (A–A'') Duf and Pyd staining in *pyd* attenuated larval nephrocytes; arrows point to Duf/Pyd at SDs and arrowheads to Duf surplus at cell contacts ($n = 49N/5S$). (B and B') In *duf^{pmf1}* larval nephrocytes, Duf colocalizes with Pyd at SDs (arrows); excess of Pyd accumulates at external puncta (arrowheads; $n = 16N/4S$). (C–C'') In *duf^{sps1}* larval nephrocytes, Pyd accumulates at external puncta (arrows) and cell contacts (arrowheads, $n = 59N/5S$). (D–D'') In stage-16 *duf^{sps1}* nephrocytes, Pyd is located in external aggregates (arrowheads); the square marks the region magnified in D' and D'' ($n = 81N$). Scale bars represent 10 μ m.

few extant SDs (Fig. 2, A–A''), while a fraction of Duf accumulated at cell contacts between partially agglutinated nephrocytes (Fig. 2 A'). A reciprocal effect was observed in the hypomorphic mutant *duf^{pmf1}*; all Duf colocalized with Pyd in SDs (Fig. 2, B and B'), whereas the excess of Pyd not associated with the low levels of Duf appeared in a dotted pattern at the external membrane of nonagglutinated nephrocytes (Fig. 2, B and B'). This phenotype was aggravated in the null allele *duf^{sps1}* in which a fraction of Pyd delocalized at cell contacts between adjacent cells while most Pyd was present in aggregates at the external membrane that lacked the fingerprint-like pattern indicative of SDs (Fig. 2, C–C''). This aberrant Pyd localization was already detectable in stage 16 *duf^{sps1}* nephrocytes (Fig. 2, D–D''). Taken together, these results suggest that Pyd and Duf mutually require each other to localize at outer membranes forming SDs and that they interact in protein complexes with fixed stoichiometry. Moreover, they indicate that while Pyd can remain at the external membrane in the absence of Duf, not participating in the formation of SDs, Duf requires Pyd for its trafficking to and/or stabilization at the outer membrane through its engagement in SDs. Otherwise, it accumulates at cell contacts where, by means of its adhesive moieties, it may contribute to mediate homotypic or heterotypic cell adhesion (Galletta et al., 2004). To gain further insight into the nature of these ectopic junctions, we looked for the presence of known junctional proteins. We failed to detect the adherens junction components E-Cadherin and β -catenin. In contrast, septate junction proteins Fas3, Discs large, and Lethal giant larvae (Figs. S2, A–C), but not Coracle or Neuroglian, localized with Duf and Sns at cell contacts in *pyd* mutant nephrocytes,

indicating that the ectopic junctions could represent modified septate junctions.

Attenuation of *zo-1* in *tjp1a* morphants induces loss of SDs and favors the formation of junctional complexes between aberrantly distended podocyte processes

Inactivation of *Tjp1* in mouse podocytes affects the glomerular filtration barrier, disrupting the architecture of foot processes and losing SDs (Itoh et al., 2014). To help clarify how vertebrate ZO-1 acts on SD formation, we examined the requirement for zebrafish *tjp1a* in the pronephros. The fish pronephros is made of two nephrons whose glomeruli show the same organization and cell types as their mammalian counterparts. Since ultrafiltration starts by 48 h postfertilization (hpf), genetic or induced conditions that affect kidney function can be easily scored by the formation of pericardial edema due to protein leakage through the glomerular barrier. We used two antisense splice blocking morpholino oligonucleotides (MOs) to target *tjp1a* (Fig. S1, I and J). Injection of the MOs in one-cell embryos results in morphants showing pericardial edema at 72 hpf and additional phenotypes, such as body-axis bending, not present in WT or in embryos injected with control MOs (Fig. 3, A–C). To check whether edema was accompanied by a kidney defect, we examined a podocin-GFP line, which allows visualization of the podocyte cell bodies and major processes (He et al., 2011). Glomeruli of morphants obtained with both MOs showed consistent retraction of the podocyte processes (Fig. 3, D–E'). These defects might account for glomerular barrier dysfunction leading to the observed pericardial edema. Congruently, TEM analysis of morphant glomeruli

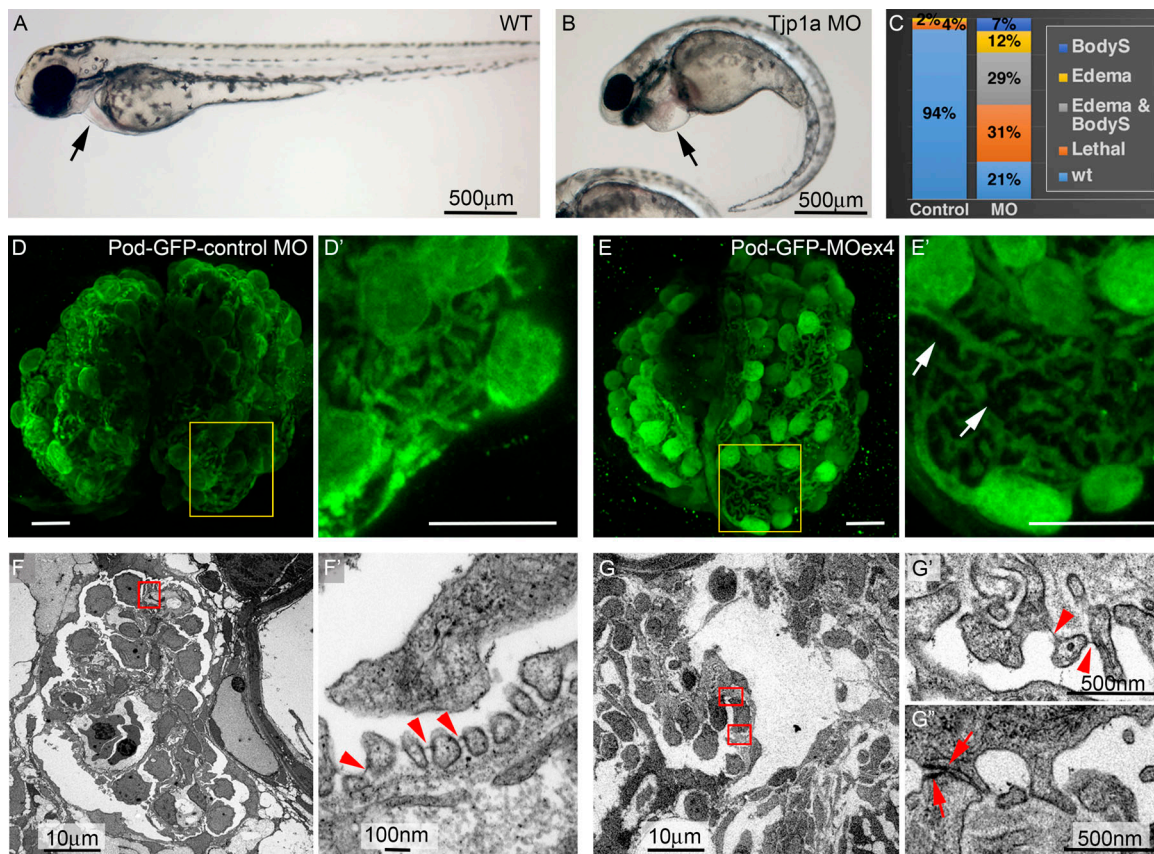


Figure 3. Tjp1a is required for SD stability in zebrafish. (A and B) WT and *tjp1a*MOex4 72-hpf larvae showing pericardial edema (arrow in B, compare to A) and body-axis curvature (BodyS) in the morphant. (C) Quantification of morphant phenotypes ($n = 82$ and 215 for control MO and MOex4). (D–E') z-projections of 96-hpf control MO*pod-GFP* (D and D') and MOex4*pod-GFP* (E and E') whole-mount glomeruli stained for GFP reveal wider gaps due to retraction of foot processes in the morphant (arrows in E', compare to D'; $n = 7$). (F–G'') TEM images of glomeruli (F and G) and filtration barrier (F', G', and G'') in control MO *pod-GFP* (F and F') and MOex4 *pod-GFP* 5 dpf larvae (G–G''). Arrowheads point to the regular array of foot processes and SDs in the control (F'; $n = 2$) and scarcity of SDs in the morphant (G'; $n = 2$). Arrows in G'' point to junctional complexes between abnormally broad processes (7 junctions per ultrathin glomerular section; $n = 3$, versus 0.3 in the controls; $n = 3$). White scale bars represent $10 \mu\text{m}$.

showed a reduced number of SDs and the presence of widened processes joined by electron-dense material reminiscent of occludens junctions (Fig. 3, F–G''). These findings confirm that vertebrate ZO-1 is required for podocyte function. Moreover, they suggest that ZO-1 promotes the formation of SDs at the expense of occludens junction-like complexes that otherwise appear between flattened podocyte processes, a phenotype reminiscent of *pyd* phenotypes in *Drosophila* (Fig. 1).

The isoform of Pyd contributing to SDs is distinct from isoforms acting on epithelial tissues

Multiple isoforms of ZO-1 exist in vertebrates that differ in the alternative inclusion of an 80-amino acid domain called α not included in the isoforms that accumulate in podocytes (Balda and Anderson, 1993). Similarly, alternative splicing and promoter usage give rise to several Pyd isoforms in *Drosophila* (Fig. 4; <https://flybase.org>). However, it is not known whether these isoforms play different roles during development. To gain further insight into this issue, we examined the ability of several Pyd isoforms to rescue *pyd* null phenotypes in nephrocytes. We first assayed Pyd-B, which rescues all ectodermal phenotypes described for *pyd* (Seppa et al., 2008; Djiane et al., 2011), and

Pyd-C, which lacks exon 12 that encodes a 78-amino acid peptide, similar in size, but not primary structure, to the mammalian α domain (Wei and Ellis, 2001). They did not rescue the *pyd* phenotype in nephrocytes either alone or in combination (Fig. S2, D–F). Moreover, although Pyd-B and Pyd-C accumulate at adherens junctions of epithelial cells (Wei and Ellis, 2001; Djiane et al., 2011), in nephrocytes Pyd-B failed to localize to the membrane and Pyd-C, while localized to the membrane, did not contribute to SDs (Fig. S2, D and F), suggesting that other isoforms not studied so far performed Pyd function in nephrocytes.

All Pyd isoforms share a core region containing three PDZ domains, one SH3 domain, and one guanylate pseudokinase domain but differentially include one CC, α , Pro-rich, or Zu5 domain (Fig. 4; <https://flybase.org>). Examination of available RNA-seq data generated from nephrocyte-enriched samples (Gill et al., 2015) revealed that in addition to the common exons, *pyd* transcripts predominantly include exon 5 that encodes a CC domain and exon 11, encoding a 372-amino acid stretch with no putative protein domains that introduces a stop codon. Thus, isoforms that include exon 11 lack α , Pro-rich, and Zu5 domains. In contrast, exons 5 and 11 are marginally represented in samples from epidermal tissues such as imaginal discs (Flegel et al.,

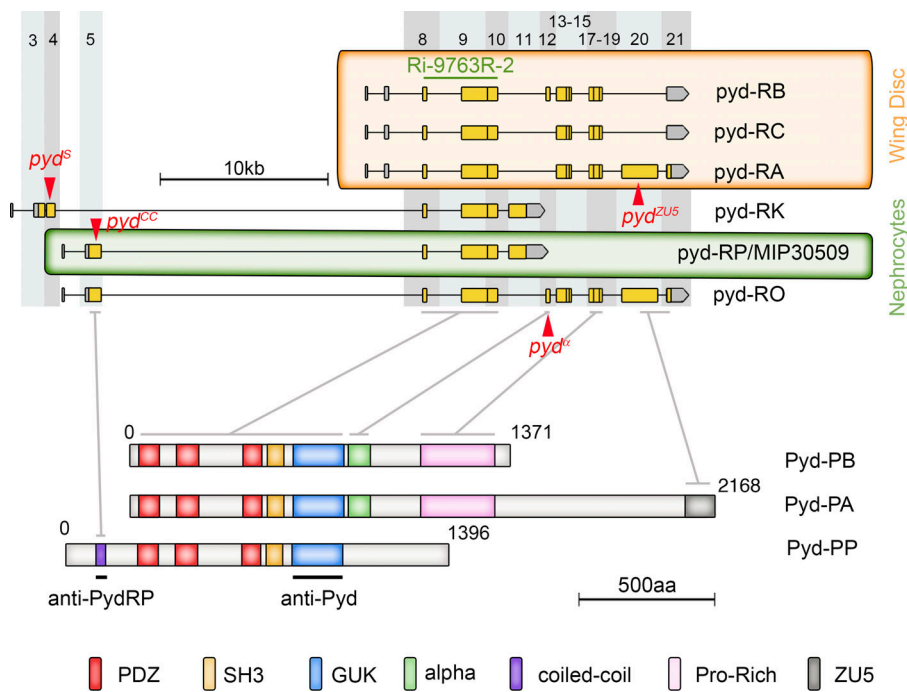


Figure 4. Pyd isoforms and protein domains. Scheme of some relevant *pyd* transcripts (adapted from flybase GBrowse) and protein isoforms showing the position of novel generated mutations (red triangles), the region targeted by the UAS-RNAi 9763R-2, and the position of the protein regions used as epitopes to raise specific antibodies. The gray columns approximately indicate coding exons, and the lines show the equivalence between exons and protein domains. Predicted isoforms Pyd-A to Pyd-C are enriched in wing discs and Pyd-P in nephrocytes.

2016). Congruently, a novel antibody raised against exon 5 recognized Pyd isoforms present in nephrocytes, but not in epithelial tissues (Fig. S3, G-I'). Thus, the described exonic composition, which corresponds to cDNA MIP30509 and that we have named Pyd-P, is probably the main isoform expressed in nephrocytes (Fig. 4).

To test this hypothesis, we generated novel *pyd* mutants, namely, *pyd^S*, *pyd^α*, *pyd^{ZUS}*, and *pyd^{CC}*, which encoded truncated proteins, devoid of different domains (Fig. 4; <https://flybase.org>, FB2018_02). The novel *pyd* mutants were homozygous viable, but whereas *pyd^S*, *pyd^α*, and *pyd^{ZUS}* exhibited the extra-bristle phenotype previously described for null alleles (Chen et al., 1996; Djiane et al., 2011), *pyd^{CC}* did not (Fig. S3, A-C). Interestingly, *pyd^S* and *pyd^α* mutants had no obvious nephrocyte phenotype (Fig. S3, E-F'), and *pyd^{ZUS}* nephrocytes, while slightly agglutinated, displayed a normal density of SDs (Fig. 5, A-B'). In contrast, *pyd^{CC}* nephrocytes exhibit the same phenotype as *pyd^{ex147}*, namely, strong agglutination with electron-dense regions at membranes contact sites, thickening of the BM, and complete absence of SDs (Fig. 5, C-D'). Moreover, introducing Pyd-P in both *pyd^{CC}* and *pyd^{ex147}* nephrocytes rescued the phenotype almost to completion, leading to recovery of labyrinthine channels and SDs (Fig. 5, E-F'), although retaining a subtle agglutination phenotype. This suggested that the ability of Pyd-P to rescue SDs relies on the presence of the CC domain. In fact, introduction of a Pyd-P protein without the CC domain (Pyd-ΔCC) in *pyd^{ex147}* nephrocytes failed to induce SD formation (Fig. 5, G and G'). In contrast, a Pyd-P protein lacking the C-terminal region but retaining the CC domain (Pyd-ΔCt) kept the ability to partially rescue SDs (Fig. 5 H), although the lack of the C-terminal region has a clear impact on Pyd-P function, revealed by the presence of numerous subcortical vesicles containing Duf and Pyd (Fig. 5 H').

Taken together, these findings indicate that the isoforms predominant in nephrocytes, which localize at SDs and are required for their formation and stability, are functionally different from the isoforms enriched in imaginal discs, which mediate functions related to receptor trafficking, adhesion, and signaling in epithelia (Seppa et al., 2008; Djiane et al., 2011). In addition, we found that overexpression of Pyd-B, which rescued the extra-bristle phenotype of *pyd^{ex147}* (Fig. S3, D and J), had no phenotypic effect when expressed in the wing disc (*ap-Gal4*), whereas similar overexpression of Pyd-P or Pyd-ΔCC induced extra-bristle phenotypes as in *pyd* mutants (Fig. S3, K and L) and overexpression of Pyd-P in eye discs (*GRM-Gal4*) induced disorganization of ommatidial cells, as in *pyd* attenuation conditions (Figs. S3, M and N; Seppa et al., 2008), suggesting that Pyd-P competes with ectodermal Pyd isoforms.

Pyd-P mediates the transition from septate-like junctions to SDs

Next, we used the TARGET system (McGuire et al., 2003) to temporally induce the expression of Pyd-P in a *pyd^{ex147}* background and examine the reversibility of *pyd* phenotype and the initial steps of Pyd-P-triggered SD formation. We verified that experimental individuals *w; tub-Gal80^{ts}/UAS-Pyd-P; pros-Gal4, pyd^{ex147}/pyd^{ex147}* continuously cultured at the permissive temperature (17°C; OFF state) exhibited the *pyd^{ex147}* null phenotype (Fig. S4 A), whereas at the restrictive temperature (29°C; ON state) the rescue phenotype (Fig. S4 B) was similar to that described in Fig. 5 E. Additional controls (mid-second larval stage kept 72 h at 29°C) showed a slight reduction in the density of SDs (Fig. S4 C).

To assay the continuous requirement of Pyd for SD stability, individuals cultured at 29°C in the presence of Pyd-P were transferred at 17°C for increasing time intervals before examining the larval nephrocytes. Only after 5 d in the absence of newly synthesized Pyd could we find phenotypes similar to

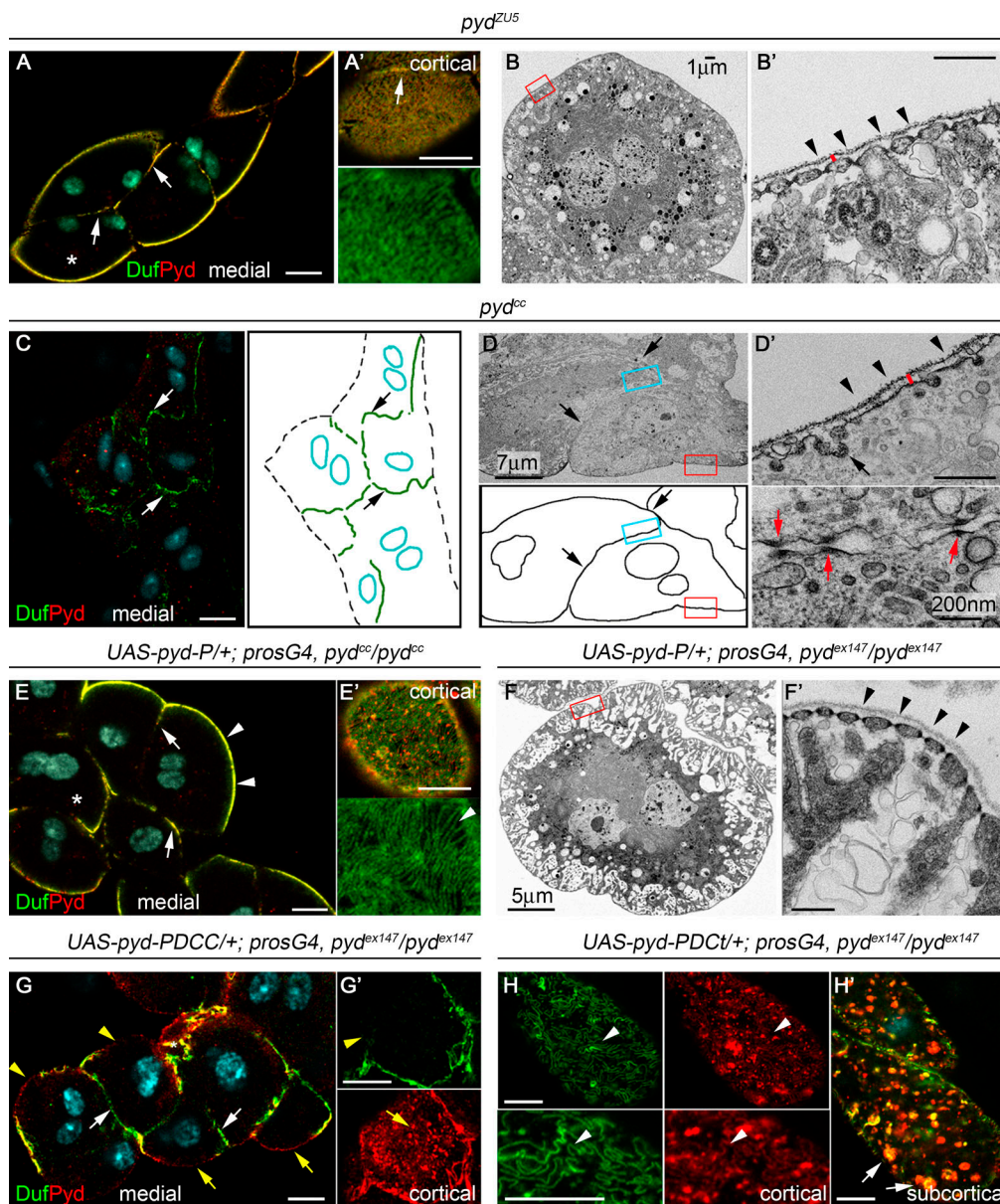


Figure 5. SD formation requires the CC domain of Pyd-P. (A–B') Confocal (A and A', $n = 150\text{N}/10\text{S}$) and TEM images (B and B') of larval *pyd^{ZU5}* nephrocytes showing Duf and Pyd at cell junctions (arrows) and normal density of SDs (arrowheads in B'). **(C–D')** Confocal (C; $n = 147\text{N}/12\text{S}$) and TEM (D and D') images and schemes of larval *pyd^{CC}* agglutinated nephrocytes. Arrows point to cell contacts, arrowheads in D' to absence of SDs, red arrows in D' to junctional complexes, and the red bar to thickening of the BM (compare to B'). **(E–F')** *Pyd-P* rescues the lack of SDs in *pyd^{CC}* (E and E', $n = 85\text{N}/7\text{S}$) and *pyd^{ex147}* (F and F', $n = 72\text{N}/6\text{S}$) mutants (arrowheads). Arrows in E point to Duf and Pyd at junctions between slightly agglutinated nephrocytes. **(G–H')** Confocal sections of larval *pyd^{ex147}* nephrocytes expressing *Pyd-P* lacking the CC (G and G') or the C-terminal (H and H') domains. *Pyd-PΔACC* ($n = 86\text{N}/9\text{S}$) fails to rescue SDs formation (yellow arrowheads and arrows mark absence of Duf and presence of Pyd in aggregates at the cortical region). White arrows in G point to Duf at cell junctions. *Pyd-PΔCt* ($n = 73\text{N}/6\text{S}$) promotes SD formation (arrowheads in H) and induces accumulation of Duf/Pyd-containing vesicles (arrows in H'). Asterisks indicate the nephrocytes shown at higher magnification. Unless otherwise indicated, black and white scale bars represent 500 nm and 10 μm , respectively. See also Fig. S1.

those produced by *Pyd* attenuation, including agglutination (Fig. S4, D–G"). These results reveal that SDs are structurally very stable (up to 5 d) and confirm that Duf localizes to ectopic junctions when it is not associated with *Pyd*.

Then, experimental animals grown at 17°C were shifted to 29°C to induce *pyd-P* expression for different intervals before examination of larval nephrocytes (Fig. 6 A). After 6 h at 29°C, in 80% of the nephrocytes, newly synthesized *Pyd* localized

predominantly in dots at the external membrane that do not contain Duf (Fig. 6, C and C'). It also accumulated with Duf at cell contacts and in large internal vesicles near these contacts (Fig. 6, C and C'). Very few SDs were observed at the cell surface and mainly on top of cell junctions (Fig. 6 F). After 15 h at 29°C, 98% of the nephrocytes showed a clear recovery. *Pyd* was still present, together with Duf, at cell junctions (Fig. 6, D–D') and in vesicles. However, the number of vesicles greatly increased, and

tub-G80ts/UAS-pyd-P; prosG4, pyd^{ex147}/pyd^{ex147}

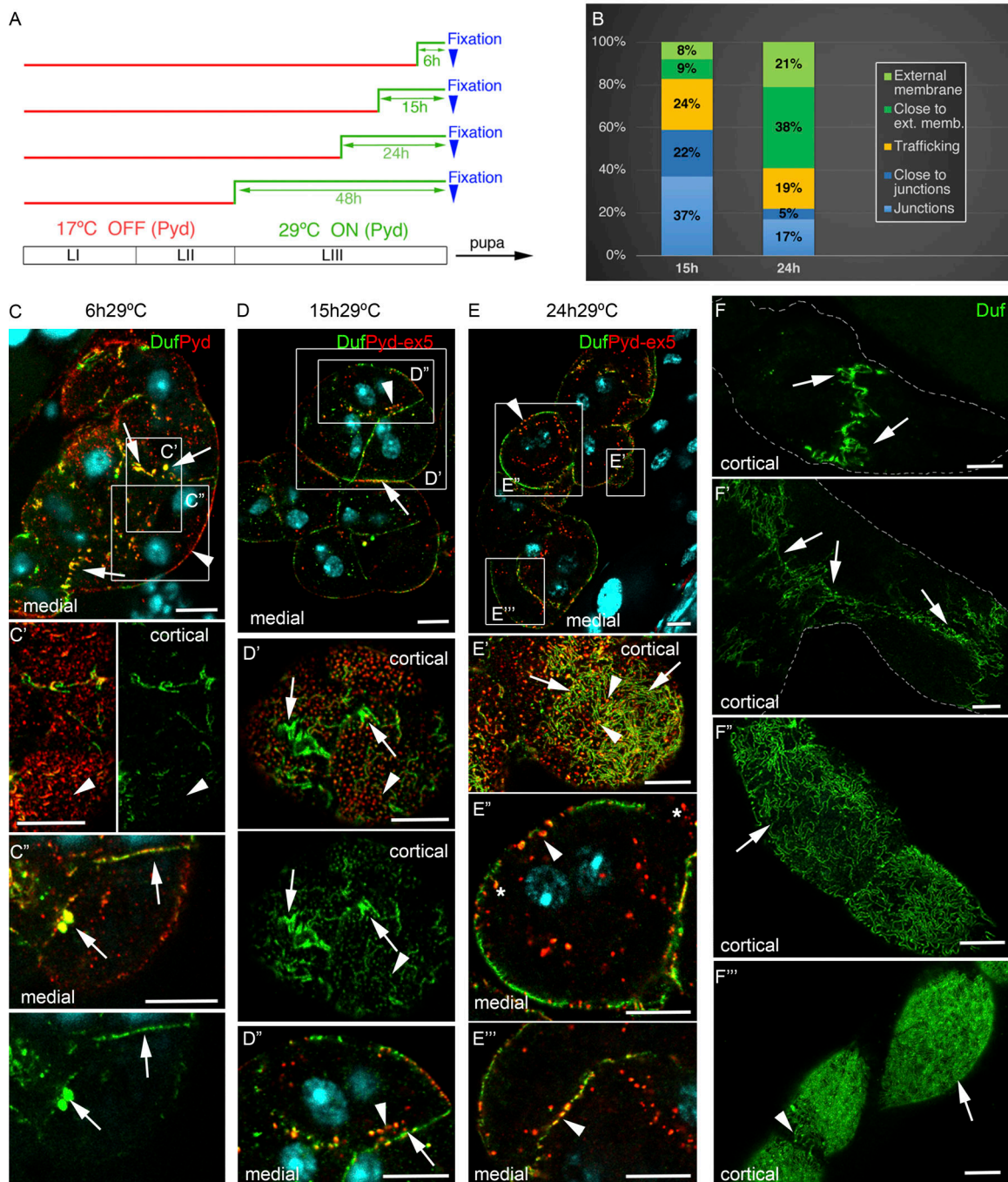


Figure 6. Pyd-P promotes junctional remodeling and formation of SDs. (A) Chart showing temporal manipulation of *pyd-P* expression in *tub-Gal80^{ts}/UAS-pyd-P; pros-Gal4, pyd^{ex147}/pyd^{ex147}* specimens. At 17°C, Gal80ts prevents Gal4-dependent activation of *UAS-pyd-P*. Nephrocytes were fixed at third-instar larval stage. LI–III refer to larval stages I–III. (B) Quantification of Duf-containing vesicles distribution at 15 h and 24 h of recovery; trafficking class includes vesicles located >2.5 μm away from membranes (*n* = 16N/3S). (C–E'') confocal sections of representative nephrocyte strings (C–E) and details of marked regions, of individuals incubated for 6 h (C–C''), 15 h (D–D''), and 24 h (E–E'') at 29°C before fixation. After 6 h at 29°C (*n* = 88N/7S), newly synthesized Pyd localizes at discrete puncta in the external membrane (arrowheads in C and C''), and colocalizes with Duf at cell junctions and in large vesicles close to the junctions (arrows in C and C''). After 15 h at 29°C (*n* = 171N/22S), Pyd colocalizes with Duf at junctions (arrows in D and D'') and in vesicles found mainly close to the junctions (arrowheads in D and D'') and in subcortical regions (arrowheads in D'). Arrows in D' point to fingerprint-like patterns, indicative of SDs found at external regions close to the junctions. After 24 h of *pyd* expression (*n* = 238N/29S), Pyd colocalizes with Duf at SDs all over the cell surface (arrows in E') at subcortical vesicles (arrowheads in E' and E''), and occasionally at cell contacts (arrowheads in E''). Asterisks mark coma-shaped vesicles. (F–F'') Nephrocyte strings showing progressive recovery of SDs over time (arrows in F'' correspond to 48 h of recovery; *n* = 112N/15S). SDs appear first close to the junctions and then extending from there to cover the whole nephrocyte surface. Scale bars represent 10 μm. See also Fig. S4.

many were found near cell contacts, appearing to emanate from the junctions (Fig. 6, D and D’; quantified in Fig. 6 B). Vesicles were also observed at the subcortical region below the external membrane (Fig. 6 D’). In addition, some SDs, mainly located at the external membrane above regions of nephrocyte contacts, were observed, and they seemed to extend from there toward the rest of the cell surface (Fig. 6, D’). After 24 h of recovery, 73% of the nephrocytes showed a normalized phenotype, with most Pyd colocalizing with Duf at SDs, which in turn cover large regions of the cell surface, although their density was much lower than in WT nephrocytes (Fig. 6, E’ and F’). In addition, Pyd and Duf were also found in vesicles, mainly subcortical (Fig. 6, B and E-E’), although some were still close to cell contacts between slightly agglutinated nephrocytes. Finally, 48 h of incubation at 29°C promoted almost complete recovery (Figs. 6 F’’ and S4 H, showing quantification of junctional complexes at 15 and 48 h of recovery). Together, these findings suggest that newly synthesized Pyd reaches the membrane and accumulates at cell-contact regions that contain Duf. This accumulation does not necessarily imply preferential sorting to specific membrane regions, since, for instance, it might reflect stabilization of Pyd after association with Duf. Subsequently, vesicles containing Duf, Pyd, and the additional SD components Sns and Cindr/CD2AP (suggesting that they might carry pre-SD complexes; Figs. 7, A and A’; and Fig. S5 A) first appear close to the cell junctions and are found after longer periods of recovery close to the external membrane, where SDs will assemble. These results suggest that in nephrocytes Pyd promotes junctional remodeling from intracellular junctions to SDs.

Pre-SD complexes accumulate in non-clathrin-coated vesicles found close to cell junctions and the external nephrocyte membrane

To investigate the mechanisms generating SDs, we focused in the Duf-Pyd-containing vesicles after 15 h of recovery. We anticipated that if their presence were connected to the formation of SDs, they would be absent when Pyd- Δ ACC is used in the rescue experiments, as was indeed the case (Fig. 7, B and D). The observation that they differed widely in size and could present tubular and coma-shaped morphologies (Fig. 6, C-E’’) was confirmed by immuno-EM analysis, revealing that Duf and Pyd were present in noncoated vesicles (Fig. 7 G) that were larger than clathrin vesicles (Fig. 7, G, H, and J) sometimes found close to cell contacts, which also accumulate Duf and Pyd (Fig. 7 G). Accordingly, coimmunostainings confirmed the presence of Duf in non-clathrin-coated vesicles during recovery that lack Rab5, Rab6, and Sec8 (Fig. 7 C and Fig. S5, D-F). As expected, Duf and Pyd also localized to SDs (Fig. 7 H) and, in addition, were found in vesicles joined by dense material mainly present inside the labyrinthine channels (Fig. 7, H-J). Finally, since formation of clathrin-independent carriers requires cytosolic organized actin, we speculated that an actomyosin motor might be responsible for the scission and traffic of the Pyd/Duf-containing vesicles and, therefore, we looked for nonmuscle myosin in the vesicles. Interestingly, we found MyoII accumulation in puncta in many of the Pyd-P-containing vesicles in rescue experiments with Pyd-P full length (Fig. 7 E) and almost complete colocalization when Pyd- Δ ACC was used (Fig. 7, F and F’).

Taken together, these findings suggest that the CC domain of Pyd-P plays a fundamental role in promoting junctional remodeling in nephrocytes. This function relies on the formation of non-clathrin-coated vesicles loaded with SD components that accumulate close to cell junctions at early stages of SD recovery and the external membrane at more advanced stages of recovery.

Discussion

A common hallmark of most congenital, acquired, and induced nephrotic conditions associated with proteinuria is a dramatic morphological transformation of podocytes, known as foot process effacement. This implies a replacement of SDs by occludens junctions, just the opposite to the sequence of events that during normal development replace tight junctions by SDs (Kriz et al., 2013; Ichimura et al., 2017), and remarks the close relationship between junctional complexes and SDs. The damage-induced morphological changes may be triggered by insults to the SD, manifested by alterations of the levels and distribution of SD components, such as the dissociation and redistribution of Neph1/ZO-1 to the cytoplasm (Rincon-Choles et al., 2006; Wagner et al., 2008) or altered junctions (Kurihara et al., 1992). More importantly, maintenance of the Neph1-ZO-1 association confers renoprotective effects to podocytes (Macconi et al., 2000). However, the way the Neph1-ZO-1 interaction impacts the formation and maintenance of the SD is not understood. The Neph1-ZO-1 (Duf/Pyd) association is conserved in flies (Weavers et al., 2009); hence, in the present study, we use the nephrocytes of *Drosophila* to analyze the role of *pyd* in the formation and stability of the SD.

Pyd is expressed and required in nephrocytes to form SDs

Several aspects of *pyd* expression and distribution uncovered in this work are informative about its function in nephrocytes, revealing a requirement of Pyd for Duf translocation toward the external membrane and for SD assembly. First, the onset of *pyd* expression is delayed with respect to *duf* expression and anticipates the appearance of the first SDs. Second, Pyd always colocalizes with Duf in nephrocytes, and they distribute in a fingerprint-like pattern at the external membrane that corresponds to rows of SDs. Third, in *pyd* mutants, SDs do not form and Duf accumulates at junctional complexes between adjacent nephrocytes. Fourth, a reduction in the levels of Pyd results in all Pyd available to colocalize with Duf at SDs, while the excess of Duf remains at cell contacts. This distribution of Duf resembles the WT situation at embryonic stage 16 (Fig. 1 A), when Pyd levels may also be limiting and Duf localizes with Pyd at SDs and with the septate junction component Fas3 at cell contacts, where it might contribute to cell adhesion. Fifth, in *duf* mutants, Pyd reaches the external membrane, but it never shows the fingerprint-like distribution indicative of SDs. If this hypothesis is correct, then one would expect anticipation of SD formation by earlier Pyd expression in nephrocytes. Even though we have not checked ubiquitous expression of Pyd-P, which might be detrimental, we found that with *Sns-GAL4*, which does not anticipate expression but increases Pyd-P levels, all Duf prematurely

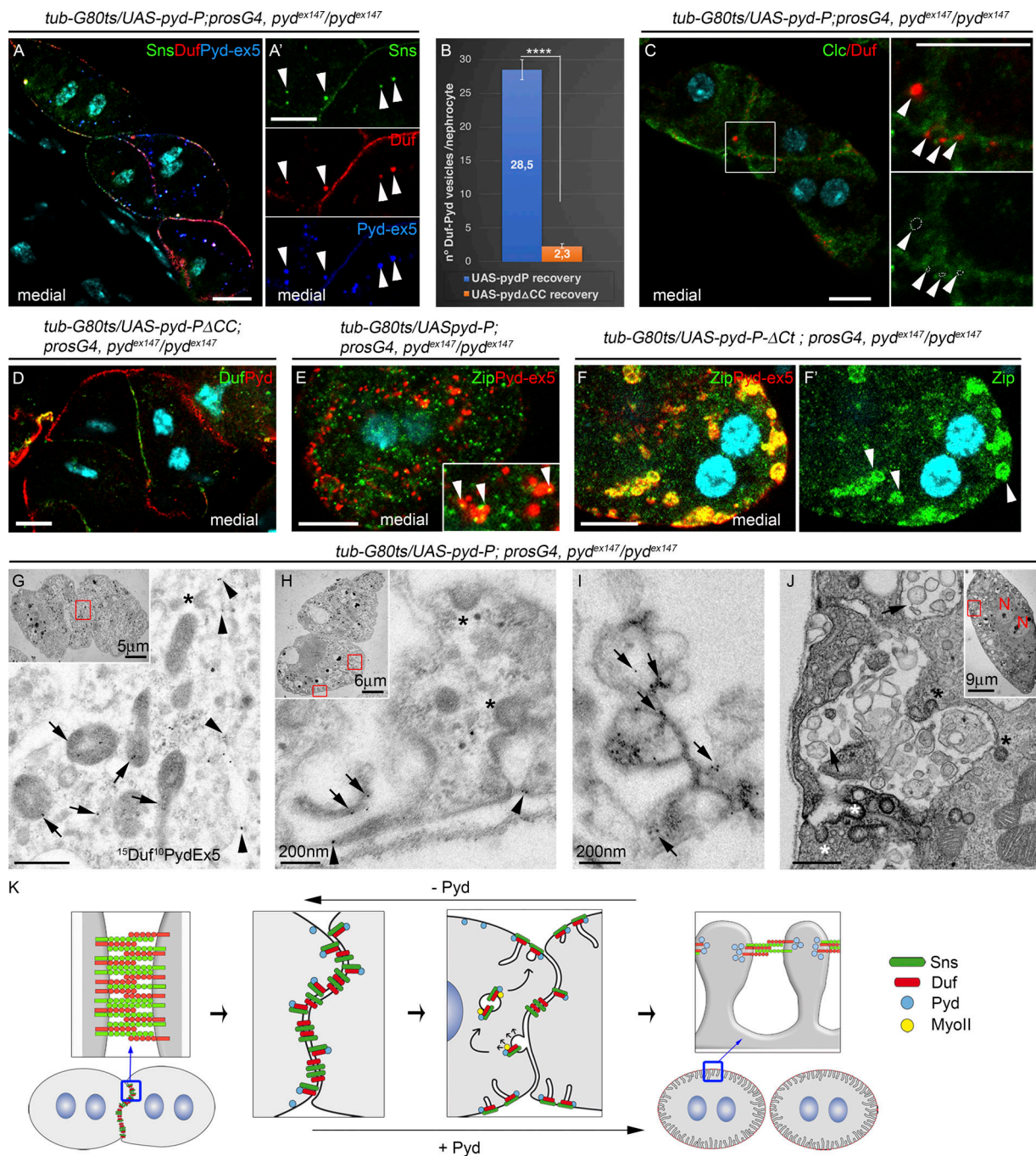


Figure 7. SD components accumulate in noncoated vesicles near cell junctions and in the external membrane. (A and C-F') Confocal images of representative *pyd^{ex147}* larval nephrocytes fixed after 15 h (6 h for C) of recovery by expression of *UAS-Pyd-P* (A, C, and E), *UAS-Pyd- Δ CC* (D), or *UAS-Pyd- Δ PdCt* (F) stained with the indicated antibodies. Vesicles (arrowheads) in A and A' contain Duf, Sns, and Pyd-P. Duf accumulates in vesicles devoid of clathrin (arrowheads in C; $n = 57N/8S$). MyoII is detected in puncta in many Pyd-P-containing vesicles (arrowheads in E; the number of MyoII-containing vesicles is significantly reduced by inversion of the green channel, discarding the possibility of random colocalization) and in all Pyd- Δ Ct vesicles (F and F'). **(B and D)** No vesicles are formed after expression of Pyd- Δ CC ($n = 63N/7S$ and $52N/8S$ for Pyd-P and Pyd- Δ CC). Error bars in B indicate SEM; ****, $P < 0.0001$ (two-tailed unpaired t test). **(G-J)** TEM images of *pyd^{ex147}* larval nephrocytes after 15 h of recovery with Pyd-P (G-I) are immunogold stained for Duf and Pyd-ex5. Duf and Pyd-P accumulate at junctions (arrowheads in G), in noncoated irregular-shaped vesicles (arrows in G) larger than clathrin-coated vesicles (asterisks in G, H, and J), at the SDs (arrowheads in H), and in vesicles connected by electron-dense material inside the channels (arrows in I and J). **(K)** Scheme describing nephrocyte junctional remodeling driven by Pyd-P. In the absence of Pyd, homo- and heterotypic interactions between Duf and Sns might contribute to nephrocyte agglutination. Association of newly synthesized Pyd with Duf at cell contacts favors cis interactions of Duf and Sns in preassembled SD complexes that are sorted into noncoated vesicles. An actomyosin motor is likely involved in trafficking of the vesicles toward the external membrane, where they deliver their cargoes to form SDs. A fall in the levels of Pyd would induce the disassembly of SDs with concomitant changes in Duf-Sns association properties and promote nephrocyte agglutination. Unless otherwise indicated, white and black scale bars represent 10 μ m and 500 nm, respectively.

mobilizes from cell contacts before stage 16, suggesting that Pyd drives the transition of Duf toward SDs in normal development. The fact that nephrocytes remain in close contact in this situation suggests that Duf is not the sole protein mediating nephrocyte adhesion at this stage. Future experiments will address the role of earlier expression of Pyd-P on the onset of SD formation. Conversely, the association of Pyd with Duf is not required for Pyd trafficking but is needed for the remodeling of junctional complexes into SDs. In addition, since the agglutination of nephrocytes in *pyd* mutants, which involves the transition from SDs to septate-like junctions, is a reversible process (Figs. 6 and S4), it highlights the importance of the Duf-Pyd association to form SDs and also preserve them.

SD formation specifically requires the Pyd-P isoform

Pyd gives rise to multiple proteins due to differential splicing. We found that Pyd-P is the main isoform required in nephrocytes, which differ from Pyd-B, the isoform active in epithelial tissues, in the differential inclusion of the α and the C-terminal Pro-rich domains in Pyd-B, and the N-terminal CC motif in Pyd-P, suggesting that their specificity likely relies on the distinct protein domains. Previous studies identified Pyd-B α and Pro-rich domains as required for the interaction with Su(dx), a protein involved in regulating Notch trafficking (Djiane et al., 2011). Since Notch activity is important for the selection of sense organ precursors, the lack of interaction with Su(dx) likely contributes to the extra-bristle phenotype observed in most *pyd* alleles and explains the normal bristle pattern of *pyd^{CC}*. In addition, the Pyd-B Pro-rich domain is required for its targeting to adherens junctions (Djiane et al., 2011) and association with Cortactin (Katsube et al., 1998) and Canoe (Takahashi et al., 1998), both of which are involved in organizing the actomyosin cytoskeleton at adherens junctions. In agreement, Cortactin and Canoe are not required for SD formation (Fig. S5, B and C).

Duf and Sns belong to a group of evolutionary conserved proteins of the immunoglobulin superfamily that participate in many cell processes involving heterotypic cell adhesion. During myoblast fusion, these proteins organize the actin cytoskeleton around the adhesion foci to increase myoblast adhesion, and they do so by engaging specific intracellular adaptors (Kim et al., 2015) not present in nephrocytes. Nephrocytes are the sole cells in the fly that coexpress Duf and Sns, and therefore, their intracellular association could modify the range of possible adaptors recruited to organize the nephrocyte cytoskeleton. Our results support this hypothesis and point to Pyd-P as one such adaptor. Hence, pan mesodermal ectopic expression of Pyd-B or Pyd-P has no effect on myoblast fusion (Fig. S3, O and P). However, the Duf-Pyd association is necessary for preserving the nephrocyte architecture and requires the Pyd-P CC N-terminal domain (Fig. 7) that may interact with a different constellation of intracellular partners, thus providing specificity in the cellular response to Pyd. The dominant-negative phenotypes observed when Pyd-P is ectopically expressed in epithelia (Fig. S3) might be explained on the basis of Pyd-B and Pyd-P recruiting a different set of downstream adaptors.

Thus, Pyd-P could directly compete with ectodermal Pyd isoforms for binding to common partners through the PDZ and SH3 domains, but it would be unable to organize the correct platform required for proper signal transductions at adherens junctions.

A mechanism for Pyd-P-driven junctional remodeling in nephrocytes

The recovery experiments provided information about a possible mechanism for Pyd-P-driven junctional remodeling in nephrocytes (Fig. 7 K). Starting from a situation without Pyd, with Duf and Sns engaged in mediating cell adhesion, provision of Pyd allowed recapitulating the sequence of steps leading to SD formation. The first step in SD formation, stimulated by binding of Pyd-P to Duf, might entail the induction of membrane bending and invagination followed by vesiculation with uptake of SD components, which requires the presence of the Pyd-P CC domain. TEM analyses revealed that SD proteins are contained in light-density uncoated vesicles, which vary in size and shape, suggesting that this process must depend on clathrin-independent carriers. While clathrin-independent endocytosis is not well described at the molecular level, it is known to mediate removal or recycling of many membrane receptors, and in many instances, actin-driving forces seem to play important roles in scission of the endocytic carriers (Ferreira and Boucrot, 2018). We have not investigated how association of Pyd with Duf might induce vesiculation, but a possible mechanism could be based on Pyd facilitating Duf-Sns clustering in cis versus preferential interactions among adjacent cells. Binding of Pyd could also provide a link with the actomyosin cytoskeleton and facilitate vesicle scission and trafficking. In this context, we found nonmuscle myosin associated with some or all the Pyd-containing vesicles during recovery, suggesting that an actomyosin motor is at work in the process. A second step in the process could involve vesicle trafficking and local delivery of cargoes at the external membrane in contact with the BM. Thus, at short recovery times, vesicles loaded with SD proteins are more abundant close to cell contacts, later at subcortical regions above them, and still later all over the subcortical region. Accordingly, SDs first appear near the intracellular junctions and seem to extend from there to cover the whole nephrocyte surface. During the third step of the process, the accumulation of pre-SD complexes at the external membrane could facilitate the assembly of SDs. We speculate that Src64B-mediated phosphorylation of Duf, which has been shown to regulate its binding to Dock/Nck (Tutor et al., 2014), together with local enrichment of other cortical actomyosin regulators, might play a fundamental role in the generation and stabilization of SDs, allowing the formation of labyrinthine channels. Remarkably, vesicles loaded with SD components are also observed during normal embryogenesis close to the external nephrocyte membrane where SDs are formed (Fig. S4 I).

Our study reveals salient parallels between SD formation in flies and vertebrates and suggests that similar mechanisms for junctional remodeling might be at work in both systems. First, Pyd, a component of both adherens junctions and SDs, is absolutely required for Duf localization at the external nephrocyte

membrane. Similarly, dissociation of the Neph1-ZO-1 complex induces delocalization of Neph1 from the podocyte membrane (Kurihara et al., 1992; Rincon-Choles et al., 2006; Wagner et al., 2008). Second, the transition from junctional complexes to SDs is a reversible process both in flies and vertebrates. Third, we find that Pyd-P induces formation of SDs, and the mobilization of Duf from cell junctions to the SDs therefore regulates junctional remodeling. Our results, together with evidence obtained in mice (Itoh et al., 2014), indicate that attenuation of *tjp1a* leads to fewer SDs and more occludens-type junctions between adjacent podocytes, suggesting that Tjpl1/ZO-1 also induce junctional transitions in podocytes.

Materials and methods

Experimental models

Drosophila

The following fly strains were used in this work: WT Oregon R, *pyd^{ex147}*, *UAS-GFPpydΔex6(RC)*, *UAS-GFPpydRB* (Djiane et al., 2011), *UASpydRFPexon6* (Seppa et al., 2008), *Df(1)Duf^{spst}* (Weavers et al., 2009), *prospero-GAL4*, *ap-GAL4* (a gift from C. Doe, Howard Hughes Medical Institute, Eugene, OR), *sns-GCN-GAL4* (Zhuang et al., 2009), *actin-GAL4*, *tubulin-GAL80^{ts20}*, *UAS-RNAi-cortactin* TRIP.GLC01362 (Bloomington Drosophila Stock Center), *P{XP}kirre^{d06226}*, *PBac{WH}kirre^{f05766}* (Exelixis, Harvard Medical School), *UAS-RNAi-cno* (Slováková and Carmena, 2011), *UAS-RNAi-pyd* (9763R-2, NIG-FLY; National Institute of Genetics, Japan), *l(2)gl^{CB02331}* (Buszczak et al., 2007), *Yrab5*, *Yrab6* (Dunst et al., 2015), *pyd^{CC6}*, *pyd^{ZU5-2}*, *pyd^{S10}*, *pyd⁹*, *Df(1)Duf^{f^mfl}*, *UASattB-pyd-P*, *UASattB-pyd-PΔCt*, and *UASattB-pyd-PΔCC* (this study; see below). Unless otherwise specified, flies were maintained under standard conditions at 25°C. To attain complete silencing of *pyd*, *sns-GCN-Gal4* females were crossed to *UAS-RNAi-9763R-2* males, and to obtain partial *pyd* attenuation (as in Fig. 2), individuals resulting from crossing *tubGAL80^{ts}*; *pros-Gal4* females to *UAS-RNAi-9763R-2* males were grown at 17°C until the third-instar larval stage and switched at 29°C for 6 h before fixation.

Zebrafish

The *Danio rerio* strains *Tuebingen*, *AB*, and *Tg-podocin:GPF* (He et al., 2011) were maintained and raised according to standard procedures described elsewhere (Westerfield, 2000).

Materials

Antibodies

Guinea pig anti-Duf extracellular (1:100; Weavers et al., 2009), mouse anti-Fas3 (1:10), mouse anti-Discs large (1:25; AB-528238 and AB-528203; Developmental Studies Hybridoma Bank), guinea pig anti-Sec8 (1:1,000; Beronja et al., 2005), rabbit anti-Clc (1:100; Heerssen et al., 2008), rabbit anti-GFP (1:300; A-6455; Thermo Fisher Scientific), rabbit anti-Zip (1:50; Kiehart and Feghali, 1986), rabbit anti-Cindr (1:400; Haglund et al., 2010), rabbit anti-Pyd (1:100), rat anti-PydEx5 (1:200), and rabbit anti-Sns ecto (1:100; this study). Alexa Fluor 488, 555, and 647 (Thermo Fisher Scientific) and 10-nm and 15-nm gold-conjugated (British Biocell International) secondary antibodies were used.

Oligonucleotides

The following oligonucleotides were used: *pydCC-gRNA-TOP*: 5'-CTTCTATAGACCCTATCCGCGATT-3', *pydCC-gRNA-BOTTOM*: 5'-AAACAATCGCGGATAGGGTCTATA-3', *pydZU5-gRNA-TOP*: 5'-CTT CGACCGTAGACGATTCTATC-3', *pydZU5-gRNA-BOTTOM*: 5'-AAACGATAGAATCGTCTACGGGTC-3', *pydα-gRNA-TOP*: 5'-CTT CTGCATACGAGAGTCGGGATG-3', *pydα-gRNA-BOTTOM*: 5'-AAA CCATCCCAGCTCTCGTATGCA-3', *pydS-gRNA-TOP*: 5'-CTTCCGATC CGTAGCCATTTCGTAG-3', *pydS-gRNA-BOTTOM*: 5'-AAACCTACG AATGGCTACGGATCG-3', *pydRO5'*: ACGTTGCGTATATAGGGGCG-3', *pydRO3'*: 5'-GTGTGCAAGCAACCTACAGC-3' (Sigma-Aldrich); control MO: 5'-CCTCTTACCTCAGTTACAATTATA-3', Lissamine, MOex4: 5'-GGATGATGTGATGCTGTTAACTTAC-3', MOex5: 5'-TGC GGATAGTCTGAATGAAGAATCA-3' (Gene Tools, LLC), *Tjpl1a-5'*: 5'-GTACAACAATGGAGGAAACTG-3', and *Tjpl1a-3'*: 5'-CAACGTCTC CCTCTTGATG-3'.

Clones and chemicals

The following clones were used: EST clone (*pyd*): MIP30509 (Roy et al., 2010), EST clone (*pyd*): LD43161 (BDGP, FBcl0165073), and cDNA clone (*duf*): NB3 (Ruiz-Gómez et al., 2000). The following chemicals were used: 1-phenyl-2-thiourea (P7629-10G; Sigma-Aldrich) and ethyl3-aminobenzoate methanesulfonate salt (A5040-25G; Fluka).

Method details

In situ hybridization and immunohistochemistry

Whole-mount in situ hybridization with digoxigenin-labeled RNA probes was done following standard protocols with minor modifications. Briefly, dechorionated embryos were fixed for 20 min in 4% PFA in PBS, methanol devitellinized, postfixed in 4% PFA in PBS, rinsed in PBT (PBS and 0.1% Tween-20), pre-hybridized in hybridization solution (50% Formamide, 4× SSC, 1× Denhardt's, 250 μg/ml salmon testis DNA, 50 μg/ml heparin, and 0.1% Tween 20) for 1 h at 55°C, and hybridized with the digoxigenin-labeled probe overnight (o/n) at 55°C in hybridization solution. Hybridized embryos were washed in PBT, incubated for 2 h at RT with anti-Dig-AP antibody, washed in PBT, rinsed in AP buffer (100 mM Tris-Cl, pH 9.5, 100 mM NaCl, 50 mM MgCl₂, and 0.1% Tween20), and developed in AP developing solution (AP + NBT and X-Phosphate) at 37°C in dark.

For immunohistochemistry in *Drosophila* samples, hot fixation was routinely used. Dissected larval nephrocytes and dechorionated embryos were fixed for 5 s in wash solution (0.7% NaCl and 0.05% Triton X-100) at 90°C and immediately transferred to ice-cold 0.7% NaCl before proceeding with devitellination (for embryos) and blocking of the samples in PBT-BSA (PBS + 0.3% Triton X-100 + 1% BSA) for 30 min at RT. Samples were incubated with primary antibodies in PBT-BSA o/n at 4°C, washed in PBT, incubated with secondary fluorescent antibodies 2 h at RT in dark, washed in PBT, rinsed in PBS, and mounted on microscope slides with Vectashield mounting medium (Vector Laboratories). Zebrafish samples for immunohistochemistry were fixed o/n at 4°C in 4% PFA in PBS, washed in PBS, permeabilized 20 min at -20°C in acetone, and washed in PBS at RT. Fixed embryos were incubated in 1% SDS in PBS 15 min at RT, washed in PBS, and blocked for 2 h at RT in blocking solution

(0.6% PBT, 10% fetal serum, and 1% DMSO), incubated o/n at 4°C with primary antibody in 0.6% PBT 2% fetal serum and 1% DMSO, washed with 0.6% PBT, incubated for 2 h at RT with secondary antibody in blocking solution, washed in PBT and rinsed in PBS, and mounted in Vectashield. Probes and antibodies are listed in the Materials section. Primers pydRO5' and pydRO3' were used for the generation of a *pyd*-P-specific digoxigenin-labeled probe.

Confocal and electron microscopy

Confocal microscopy and TEM were performed following standard techniques modified as in [Weavers et al. \(2009\)](#). For immuno-EM, dissected larval nephrocytes were fixed in 4% PFA, embedded in gelatin, cryosectioned, and incubated with anti-Duf (1:25), anti-Pyd (1:10), and anti-Pyd-ex5 (1:50) antibodies. Samples for electron microscopy were observed in a Jem1010 (JEOL) instrument working at 80 kV with a TemCam F416 (TVIPS) camera and EMenu software. Fluorescent images were acquired using a confocal LSM 710 (Zeiss) connected to an AxioImager.M2 (Zeiss) vertical microscope with 40×/1.3 or 63×/1.4 objectives, 1,024/1,024-pixel resolution, and Zeiss ZEN 2010 software. Thorax images were obtained in an Axiophot Zeiss microscope equipped with a DFC425 Leica camera mounted with a 5×/0.15 Neofluar objective using Leica Application Suite 4.9.0 software. Images were processed with Adobe Photoshop CS5 and ImageJ 2.0.0-rc-64 software. All images were obtained at RT.

Antibody production

To generate the anti-Pyd polyclonal antibody, a DNA fragment including sequences encoding the guanylate pseudokinase domain, from Gly 708 to Ala974 in EST LD43161, was cloned into the expression vector pGEX-4T-1. The anti-Sns-ecto polyclonal antibody was raised against amino acids 676–1,022 of Sns protein fused to GST. The GST-tagged fusion peptides were used to inoculate rabbits following standard protocols. To generate isoform Pyd-P-specific antibodies, a DNA fragment corresponding to coding sequence of Pyd exon 5, from Met1 to Lys240, was PCR amplified from EST MIP30509 and cloned into pET-14b. A His-tag fusion protein was expressed in *Escherichia coli*, purified under denaturing conditions by standard IMAC (immobilized metal affinity chromatography), and used to immunize rats.

Generation of novel *Drosophila* lines

Novel *pyd* alleles were generated using CRISPR-Cas9 technology, following the protocol specified in ([Kondo and Ueda, 2013](#)). The primers used to generate the gRNAs vectors targeting different *Pyd* isoforms are listed in the Materials section and were designed using the <http://www.flyrnai.org/crispr/> website. For each mutagenesis, ≥10 independent lines were sequenced. The mutants used in this study are listed in the experimental models section. Mutant *pyd*^{ZU5-2} has a deletion of five nucleotides in *pyd* exon-20, inducing a frameshift that affects predicted isoforms Pyd-PA and Pyd-PO, generating truncated proteins. *pyd*^{α9} contains an insertion of two nucleotides in exon 12 that introduces a frame shift and a premature stop codon that affects isoform Pyd-PB and predicted isoforms Pyd-PO, Pyd-PF, Pyd-PI, and Pyd-PJ. *pyd*^{CC6} contains an indel in exon 5 that causes a premature stop

Table 1. Sequences with the changes introduced in the different mutants

Mutant	Sequence (5'-3')
WT	GGTGATGACCCGTAGACGATTCATCCGGGGGCTGCCAATGAGCAGA
<i>pyd</i> ^{ZU5-2}	GGTGATGACCCGTAGACGAT-----CCGGGGGCTGCCAATGAGCAGA
WT	CGATTTCCTATTCCCCATGACCACAT--CCCGACTCTCGT
<i>pyd</i> ^{α9}	CGATTTCCTATTCCCCATGACCACATGACCCGACTCTCGT
WT	CGAGTGGAGGTACCAAATCGC----GGATAGGGTCTATACCACCAG
<i>pyd</i> ^{CC6}	CGAGTGGAGGTACCAAATAGGATAGGGATAGGGTCTATACCACCAG
WT	CGCTAATACTGGCACCATATCCTCTACGAATGGCTACGGATCGCTG
<i>pyd</i> ^{S-10}	CGCTAATACTGGCACCATATCCTC-----TACGGATCGCTG

WT from FlyBase release FB2019_01.

codon in Pyd-PP and predicted isoform Pyd-PO. Finally, *pyd*^{S10} has a deletion of 10 nucleotides in exon 3 that introduces a premature stop codon affecting isoforms Pyd-PK and Pyd-PJ. The relevant sequences with the changes introduced in the different mutants are shown in [Table 1](#).

Df(1)Duf^{pmf}, affecting the *duf* regulatory region, was generated by FLP-induced recombination using the insertions *P{XP}kirre^{d06226}* and *PBac{WH}kirre⁰⁵⁷⁶⁶* following the protocol described in [Parks et al. \(2004\)](#). The *UAS* transgenic lines *UAS-pyd-P*, *UAS-pyd-PΔCt* and *UAS-pyd-PΔCC* were obtained by site-specific transgenesis, after insertion of the full-length *pyd-P* sequence from EST MIP30509 and the specified deletions (details will be provided under request) into the pUAS-attB vector and transformation into the ZH-attP-22A line ([Bischof et al., 2007](#)).

Bioinformatics analysis of *pyd* isoforms

To identify *pyd* isoforms, we used public data from FlyBase as well as available raw RNA-seq data obtained from diverse *Drosophila* tissues. In particular, adult heart (SRR17707795, SRR17707796, SRR17707797, and SRR17707798; [Gill et al., 2015](#)), wing imaginal disc (SRR3478156; [Flegel et al., 2016](#)), midgut (SRR2930812; [Hudry et al., 2016](#)), brain (SRR1712836), and ovaries (SRR1783726). Reads were mapped to the genome using TopHat in the Galaxy platform (<https://usegalaxy.org>) and visualized with IGV browser. To examine whether the adult heart samples are enriched in pericardial cells, we checked for expression of several nephrocyte-specific genes (*dCubn*, *dAMN*, *duf*, and *sns*). All were highly expressed. RNA-seq data shows that *pyd* is a complex locus, with 5 alternative promoters and four alternative exons (11, 12, 16, and 20). Exons 11 and 16 introduce premature stop codons, whereas exon 21 is translated in two possible frames, one of them also introducing a premature stop. Importantly, the RNA-seq data shows that in the heart-pericardial cell tissue *pyd* is translated starting at exons 5 and 1. Moreover, exon 11 is highly represented in the transcriptomic data from this tissue, with only 8 reads consistent with transcripts skipping exon 11, while 111 reads indicate splicing between exons 10 and 11 and 109 reads between exon 11 and 12.

Morpholino injections

Experimental and control MOs (listed in the Materials section) were obtained from Gene Tools. MOex4 and MOex5 were designed against the splice donor and acceptor sites of exons 4 and 5, respectively, that encode part of the Tjpl1a PDZ1 domain. In all cases, one-cell-stage podocin-GFP or AB/TUE embryos were injected with 2–3 nl of 0.7 mM MOs. To verify the efficacy of the injected MOs, primers Tjpl1a-5' and Tjpl1a-3' were designed to amplify a 683-bp region between properly spliced exons 4 and 5. Analysis of WT- and MO-injected embryos was performed by RT-PCR from total RNA of 72-hpf individuals.

Statistical analysis

Statistical analysis was performed using GraphPad Prism 7.0 trial software using a two-tailed unpaired *t* test for Duf vesicle quantification (Fig. 7 B) and a two-tailed paired *t* test for zipper quantification in vesicles and quantification of junctions (Fig. S4). *P* values <0.05 were considered statistically significant (**, *P* < 0.01; ***, *P* < 0.001). Data distribution was assumed to be normal, but this was not formally tested.

Online supplemental material

Fig. S1 shows the onset of *pyd* expression in relation to that of *duf* during embryogenesis. It also shows the morpholino efficacy in depleting *tjpl1a* in the morphants. Fig. S2 shows that the septate junction components Fas3, Dlg, and Lgl accumulate at ectopic junctions in *pyd* mutant nephrocytes and that isoforms Pyd-B and Pyd-C fail to rescue the *pyd* loss-of-function phenotype in nephrocytes. Fig. S3 shows the bristle and nephrocyte phenotypes of some *pyd* mutants generated in this study, effects of overexpression of several Pyd isoforms in different tissues, and specificity of the anti-Pyd-P antibody. Fig. S4 shows some controls and the effect of temporal manipulation of Pyd-P on the stability of SDs; it also shows the quantification of junctional complexes at two time intervals during recovery and the presence of vesicles loaded with Duf and Pyd in nephrocytes during embryogenesis. Fig. S5 shows that the vesicles loaded with Duf, Sns, and Pyd that are present close to junctions at short times of recovery also contain the SD component Cindr/CD2AP, but not Rab5, Rab6, or Sec8. It also shows that attenuation of *cortactin* or *canoe* in nephrocytes has no effect on SD formation. Video 1 shows a 3D reconstruction of embryonic stage 16 WT nephrocytes stained for Duf, Fas3, and DAPI.

Acknowledgments

We thank S. Bray, M. Baron, R. Cagan, S. Abmayr, and B. He for sharing reagents; Bloomington, NIG-FLY, Exelixis, Vienna Drosophila Resource Center, and the Drosophila Studies Hybridoma Bank for providing fly stocks and antibodies; and J. Modolell, A. Ortiz, and J.F. de Celis for critical comments on the manuscript. We also thank R. Menchén and the Drosophila transgenesis and confocal and electron microscopy facilities of the Centro de Biología Molecular Severo Ochoa for technical support.

This work was supported by Ministerio de Economía y Competitividad grants BFU2013-45430P and BFU2016-79220P to M. Ruiz-Gómez and J. Culi. Institutional support from Fundación

Ramón Areces to the Centro de Biología Molecular Severo Ochoa is also acknowledged.

The authors declare no competing financial interests.

Author contributions: M. Carrasco-Rando, S. Prieto-Sánchez, J. Culi, and M. Ruiz-Gómez conceived and performed experiments and analyzed and curate data. A.S. Tutor performed experiments. M. Carrasco-Rando designed figures. M. Carrasco-Rando and J. Culi revised the manuscript, and M. Ruiz-Gómez wrote and revised the manuscript.

Submitted: 30 October 2018

Revised: 21 March 2019

Accepted: 14 May 2019

References

- Aggarwal, S.K., and R.C. King. 1967. The ultrastructure of the wreath cells of *Drosophila melanogaster* larvae. *Protoplasma*. 63:343–352. <https://doi.org/10.1007/BF01252944>
- Balda, M.S., and J.M. Anderson. 1993. Two classes of tight junctions are revealed by ZO-1 isoforms. *Am. J. Physiol.* 264:C918–C924. <https://doi.org/10.1152/ajpcell.1993.264.4.C918>
- Barletta, G.M., I.A. Kovari, R.K. Verma, D. Kerjaschki, and L.B. Holzman. 2003. Nephrin and Nephl co-localize at the podocyte foot process intercellular junction and form cis hetero-oligomers. *J. Biol. Chem.* 278:19266–19271. <https://doi.org/10.1074/jbc.M301279200>
- Beronja, S., P. Laprise, O. Papoulas, M. Pellikka, J. Sisson, and U. Tepass. 2005. Essential function of *Drosophila* Sec6 in apical exocytosis of epithelial photoreceptor cells. *J. Cell Biol.* 169:635–646. <https://doi.org/10.1083/jcb.200410081>
- Bischof, J., R.K. Maeda, M. Hediger, F. Karch, and K. Basler. 2007. An optimized transgenesis system for *Drosophila* using germ-line-specific phiC31 integrases. *Proc. Natl. Acad. Sci. USA.* 104:3312–3317. <https://doi.org/10.1073/pnas.061151104>
- Buszczak, M., S. Paterno, D. Lighthouse, J. Bachman, J. Planck, S. Owen, A.D. Skora, T.G. Nystul, B. Ohlstein, A. Allen, et al. 2007. The carnegie protein trap library: a versatile tool for *Drosophila* developmental studies. *Genetics.* 175:1505–1531. <https://doi.org/10.1534/genetics.106.065961>
- Carrasco-Rando, M., A. Atienza-Manuel, A.S. Tutor, and M. Ruiz-Gómez. 2015. Modelling Renal Development and Disease in *Drosophila*. John Wiley & Sons, Chichester, UK.
- Chen, C.M., J.A. Freedman, D.R. Bettler Jr., S.D. Manning, S.N. Giep, J. Steiner, and H.M. Ellis. 1996. Polychaetoid is required to restrict segregation of sensory organ precursors from proneural clusters in *Drosophila*. *Mech. Dev.* 57:215–227. [https://doi.org/10.1016/0925-4773\(96\)00548-5](https://doi.org/10.1016/0925-4773(96)00548-5)
- Crossley, A.C. 1972. The ultrastructure and function of pericardial cells and other nephrocytes in an insect: *Calliphora erythrocephala*. *Tissue Cell.* 4:529–560. [https://doi.org/10.1016/S0040-8166\(72\)80029-6](https://doi.org/10.1016/S0040-8166(72)80029-6)
- de Velasco, B., L. Mandal, M. Mkrtchyan, and V. Hartenstein. 2006. Subdivision and developmental fate of the head mesoderm in *Drosophila melanogaster*. *Dev. Genes Evol.* 216:39–51. <https://doi.org/10.1007/s00427-005-0029-4>
- Djiane, A., H. Shimizu, M. Wilkin, S. Mazleyrat, M.D. Jennings, J. Avis, S. Bray, and M. Baron. 2011. Su(dx) E3 ubiquitin ligase-dependent and -independent functions of polychaetoid, the *Drosophila* ZO-1 homologue. *J. Cell Biol.* 192:189–200. <https://doi.org/10.1083/jcb.201007023>
- Dunst, S., T. Kazimiers, F. von Zadow, H. Jambor, A. Sagner, B. Brankatschk, A. Mahmoud, S. Spannl, P. Tomancak, S. Eaton, and M. Brankatschk. 2015. Endogenously tagged rab proteins: a resource to study membrane trafficking in *Drosophila*. *Dev. Cell.* 33:351–365. <https://doi.org/10.1016/j.devcel.2015.03.022>
- Ferreira, A.P.A., and E. Boucrot. 2018. Mechanisms of Carrier Formation during Clathrin-Independent Endocytosis. *Trends Cell Biol.* 28:188–200. <https://doi.org/10.1016/j.tcb.2017.11.004>
- Flegel, K., O. Grushko, K. Bolin, E. Griggs, and L. Buttitta. 2016. Roles for the Histone Modifying and Exchange Complex NuA4 in Cell Cycle Progression in *Drosophila melanogaster*. *Genetics.* 203:1265–1281. <https://doi.org/10.1534/genetics.116.188581>

- Galletta, B.J., M. Chakravarti, R. Banerjee, and S.M. Abmayr. 2004. SNS: Adhesive properties, localization requirements and ectodomain dependence in S2 cells and embryonic myoblasts. *Mech. Dev.* 121: 1455–1468. <https://doi.org/10.1016/j.mod.2004.08.001>
- Gerke, P., T.B. Huber, L. Sellin, T. Benzing, and G. Walz. 2003. Homodimerization and heterodimerization of the glomerular podocyte proteins nephrin and NEPH1. *J. Am. Soc. Nephrol.* 14:918–926. <https://doi.org/10.1097/ASN.0000057853.05686.89>
- Gill, S., H.D. Le, G.C. Melkani, and S. Panda. 2015. Time-restricted feeding attenuates age-related cardiac decline in *Drosophila*. *Science*. 347: 1265–1269. <https://doi.org/10.1126/science.1256682>
- Grahammer, F., C. Schell, and T.B. Huber. 2013. The podocyte slit diaphragm—from a thin grey line to a complex signalling hub. *Nat. Rev. Nephrol.* 9:587–598. <https://doi.org/10.1038/nrneph.2013.169>
- Haglund, K., I.P. Nezis, D. Lemus, C. Grabbe, J. Wesche, K. Liestøl, I. Dikic, R. Palmer, and H. Stenmark. 2010. Cindr interacts with anillin to control cytokinesis in *Drosophila melanogaster*. *Curr. Biol.* 20:944–950. <https://doi.org/10.1016/j.cub.2010.03.068>
- Hattori, S., S. Kanda, and Y. Harita. 2011. Tyrosine kinase signaling in kidney glomerular podocytes. *J. Signal Transduct.* 2011:317852. <https://doi.org/10.1155/2011/317852>
- He, B., L. Ebarasi, K. Hultenby, K. Tryggvason, and C. Betsholtz. 2011. Podocin-green fluorescence protein allows visualization and functional analysis of podocytes. *J. Am. Soc. Nephrol.* 22:1019–1023. <https://doi.org/10.1681/ASN.2010121291>
- Heerssen, H., R.D. Fetter, and G.W. Davis. 2008. Clathrin dependence of synaptic-vesicle formation at the *Drosophila* neuromuscular junction. *Curr. Biol.* 18:401–409. <https://doi.org/10.1016/j.cub.2008.02.055>
- Helmstädter, M., T.B. Huber, and T. Hermlle. 2017. Using the *Drosophila* Nephrocyte to Model Podocyte Function and Disease. *Front Pediatr.* 5: 262. <https://doi.org/10.3389/fped.2017.00262>
- Hudry, B., S. Khadayate, and I. Miguel-Aliaga. 2016. The sexual identity of adult intestinal stem cells controls organ size and plasticity. *Nature*. 530: 344–348. <https://doi.org/10.1038/nature16953>
- Ichimura, K., S. Kakuta, Y. Kawasaki, T. Miyaki, T. Nonami, N. Miyazaki, T. Nakao, S. Enomoto, S. Arai, M. Koike, et al. 2017. Morphological process of podocyte development revealed by block-face scanning electron microscopy. *J. Cell Sci.* 130:132–142. <https://doi.org/10.1242/jcs.187815>
- Itoh, M., K. Nakadate, Y. Horibata, T. Matsusaka, J. Xu, W. Hunziker, and H. Sugimoto. 2014. The structural and functional organization of the podocyte filtration slits is regulated by Tjp1/ZO-1. *PLoS One*. 9:e106621. <https://doi.org/10.1371/journal.pone.0106621>
- Katsube, T., M. Takahisa, R. Ueda, N. Hashimoto, M. Kobayashi, and S. Togashi. 1998. Cortactin associates with the cell-cell junction protein ZO-1 in both *Drosophila* and mouse. *J. Biol. Chem.* 273:29672–29677. <https://doi.org/10.1074/jbc.273.45.29672>
- Kiehart, D.P., and R. Feghali. 1986. Cytoplasmic myosin from *Drosophila melanogaster*. *J. Cell Biol.* 103:1517–1525. <https://doi.org/10.1083/jcb.103.4.1517>
- Kim, J.H., P. Jin, R. Duan, and E.H. Chen. 2015. Mechanisms of myoblast fusion during muscle development. *Curr. Opin. Genet. Dev.* 32:162–170. <https://doi.org/10.1016/j.gde.2015.03.006>
- Kondo, S., and R. Ueda. 2013. Highly improved gene targeting by germline-specific Cas9 expression in *Drosophila*. *Genetics*. 195:715–721. <https://doi.org/10.1534/genetics.113.156737>
- Kriz, W., I. Shirato, M. Nagata, M. LeHir, and K.V. Lemley. 2013. The podocyte's response to stress: the enigma of foot process effacement. *Am. J. Physiol. Renal Physiol.* 304:F333–F347. <https://doi.org/10.1152/ajprenal.00478.2012>
- Kurihara, H., J.M. Anderson, D. Kerjaschki, and M.G. Farquhar. 1992. The altered glomerular filtration slits seen in puromycin aminonucleoside nephrosis and protamine sulfate-treated rats contain the tight junction protein ZO-1. *Am. J. Pathol.* 141:805–816.
- Macconi, D., M. Ghilardi, M.E. Bonassi, E.I. Mohamed, M. Abbate, F. Colombi, G. Remuzzi, and A. Remuzzi. 2000. Effect of angiotensin-converting enzyme inhibition on glomerular basement membrane permeability and distribution of zonula occludens-1 in MWF rats. *J. Am. Soc. Nephrol.* 11:477–489.
- McGuire, S.E., P.T. Le, A.J. Osborn, K. Matsumoto, and R.L. Davis. 2003. Spatiotemporal rescue of memory dysfunction in *Drosophila*. *Science*. 302:1765–1768. <https://doi.org/10.1126/science.1089035>
- Na, J., M.T. Sweetwyne, A.S. Park, K. Susztak, and R.L. Cagan. 2015. Diet-Induced Podocyte Dysfunction in *Drosophila* and Mammals. *Cell Reports*. 12:636–647. <https://doi.org/10.1016/j.celrep.2015.06.056>
- Parks, A.L., K.R. Cook, M. Belvin, N.A. Dompe, R. Fawcett, K. Huppert, L.R. Tan, C.G. Winter, K.P. Bogart, J.E. Deal, et al. 2004. Systematic generation of high-resolution deletion coverage of the *Drosophila melanogaster* genome. *Nat. Genet.* 36:288–292. <https://doi.org/10.1038/ng1312>
- Qin, X.S., H. Tsukaguchi, A. Shono, A. Yamamoto, H. Kurihara, and T. Doi. 2009. Phosphorylation of nephrin triggers its internalization by raft-mediated endocytosis. *J. Am. Soc. Nephrol.* 20:2534–2545. <https://doi.org/10.1681/ASN.2009010011>
- Rincon-Choles, H., T.L. Vasylyeva, P.E. Pergola, B. Bhandari, K. Bhandari, J.H. Zhang, W. Wang, Y. Gorin, J.L. Barnes, and H.E. Abboud. 2006. ZO-1 expression and phosphorylation in diabetic nephropathy. *Diabetes*. 55: 894–900. <https://doi.org/10.2337/diabetes.55.04.06.db05-0355>
- Roy, S., J. Ernst, P.V. Kharchenko, P. Kheradpour, N. Negre, M.L. Eaton, J.M. Landolin, C.A. Bristow, L. Ma, M.F. Lin, et al. modENCODE Consortium. 2010. Identification of functional elements and regulatory circuits by *Drosophila* modENCODE. *Science*. 330:1787–1797. <https://doi.org/10.1126/science.1198374>
- Ruiz-Gómez, M., N. Coutts, A. Price, M.V. Taylor, and M. Bate. 2000. *Drosophila* dumbfounded: a myoblast attractant essential for fusion. *Cell*. 102:189–198. [https://doi.org/10.1016/S0092-8674\(00\)00024-6](https://doi.org/10.1016/S0092-8674(00)00024-6)
- Sanchez-Niño, M.D., A.B. Sanz, A.M. Ramos, M. Ruiz-Ortega, and A. Ortiz. 2017. Translational science in chronic kidney disease. *Clin. Sci. (Lond.)*. 131:1617–1629. <https://doi.org/10.1042/CS20160395>
- Seppa, M.J., R.I. Johnson, S. Bao, and R.L. Cagan. 2008. Polychaetoid controls patterning by modulating adhesion in the *Drosophila* pupal retina. *Dev. Biol.* 318:1–16. <https://doi.org/10.1016/j.ydbio.2008.02.022>
- Slováková, J., and A. Carmena. 2011. Canoe functions at the CNS midline glia in a complex with Shotgun and Wrapper-Nrx-IV during neuron-glia interactions. *Development*. 138:1563–1571. <https://doi.org/10.1242/dev.056192>
- Takahashi, K., T. Matsuo, T. Katsube, R. Ueda, and D. Yamamoto. 1998. Direct binding between two PDZ domain proteins Canoe and ZO-1 and their roles in regulation of the jun N-terminal kinase pathway in *Drosophila* morphogenesis. *Mech. Dev.* 78:97–111. [https://doi.org/10.1016/S0925-4773\(98\)00151-8](https://doi.org/10.1016/S0925-4773(98)00151-8)
- Tutor, A.S., S. Prieto-Sánchez, and M. Ruiz-Gómez. 2014. Src64B phosphorylates Dumbfounded and regulates slit diaphragm dynamics: *Drosophila* as a model to study nephropathies. *Development*. 141:367–376. <https://doi.org/10.1242/dev.099408>
- Wagner, M.C., G. Rhodes, E. Wang, V. Pruthi, E. Arif, M.A. Saleem, S.E. Wean, P. Garg, R. Verma, L.B. Holzman, et al. 2008. Ischemic injury to kidney induces glomerular podocyte effacement and dissociation of slit diaphragm proteins Nephl and ZO-1. *J. Biol. Chem.* 283:35579–35589. <https://doi.org/10.1074/jbc.M805507200>
- Weavers, H., S. Prieto-Sánchez, F. Grawe, A. Garcia-López, R. Artero, M. Wilsch-Bräuninger, M. Ruiz-Gómez, H. Skaer, and B. Denholm. 2009. The insect nephrocyte is a podocyte-like cell with a filtration slit diaphragm. *Nature*. 457:322–326. <https://doi.org/10.1038/nature07526>
- Wei, X., and H.M. Ellis. 2001. Localization of the *Drosophila* MAGUK protein Polychaetoid is controlled by alternative splicing. *Mech. Dev.* 100: 217–231. [https://doi.org/10.1016/S0925-4773\(00\)00550-5](https://doi.org/10.1016/S0925-4773(00)00550-5)
- Westerfield, M. 2000. *The Zebrafish Book. A Guide for the Laboratory Use of Zebrafish (Danio rerio)*. University of Oregon Press, Eugene, OR.
- Zhuang, S., H. Shao, F. Guo, R. Trimble, E. Pearce, and S.M. Abmayr. 2009. Sns and Kirre, the *Drosophila* orthologs of Nephrin and Nephl, direct adhesion, fusion and formation of a slit diaphragm-like structure in insect nephrocytes. *Development*. 136:2335–2344. <https://doi.org/10.1242/dev.031609>